Separation control and efficiency improvement in a 2D diffuser by means of contoured cavities

A. Mariotti[a,*], A.N. Grozescu[a], G. Buresti[a], M.V. Salvetti[a]

[a] *Dipartimento di Ingegneria Civile e Industriale, Università di Pisa, Via G. Caruso 8, 56122 Pisa, Italia*

Abstract

The performance of a passive control method aimed at reducing and, possibly, eliminating boundary layer separation is evaluated by means of numerical simulation. The passive control, which consists in introducing appropriately-shaped cavities in solid walls, is applied to a plane diffuser. The Reynolds number is such that turbulence can be neglected ($Re = 500$, based on the diffuser half-width at the inlet section and the inlet velocity on the axis). A configuration characterized by an area ratio of 2 and a divergence angle of 7 degrees is chosen, so that, without the introduction of the control, the flow is characterized by a large zone of steady asymmetrical boundary layer separation. In order to reduce the separated zone and to increase the efficiency of the diffuser, a couple of symmetric contoured cavities is introduced in the diverging walls. An optimization procedure is developed to obtain the cavity geometry that maximizes the pressure recovery in the diffuser and minimizes the boundary layer separation extent. The introduction of the

*Corresponding author
Email addresses: alessandro.mariotti@for.unipi.it (A. Mariotti), annabella.grozescu@gmail.com (A.N. Grozescu), g.buresti@ing.unipi.it (G. Buresti), mv.salvetti@ing.unipi.it (M.V. Salvetti)

optimal cavities leads to an increase in pressure recovery of the order of 13% and to a strong reduction of the separation extent. This result is due to a favourable modification of the velocity and vorticity fields in the near-wall region. The most important geometrical parameters are also identified and the robustness of the control to small changes in their values is investigated. It is found that the contoured cavities are effective as long as the flow is able to reattach immediately downstream of the cavities.
Keywords: passive flow control, contoured cavities, boundary layer separation, low Reynolds diffuser

1. Introduction

Boundary layer separation can occur in many external and internal flows, which are characteristic of environmental problems as well as of industrial and engineering applications. From a practical viewpoint, due to the large energy losses often associated with boundary layer separation, a crucial issue in many technological applications is the development of methodologies to reduce or, possibly, to avoid separation (see e.g. the reviews by [1, 2]).

In the present work, we are interested in appraising the capabilities of a passive method for the control of boundary layer separation. The considered strategy is based on the introduction of appropriately-shaped cavities in the solid walls. This method combines the ideas of using, as a control device, trapped vortices (see e.g. [3–8]) and multi-step afterbodies (see e.g. [9–11]).

The trapped-vortex idea is based on the observation that the vortices forming inside cavities made in solid walls cause a higher momentum to be present in the downstream boundary layer, so that separation may be de-

layed. In this control strategy, the cavities are typically much larger than the boundary layer thickness. The trapped-vortex concept was first introduced by Ringleb [3], who proposed it for boundary layer control in both external and internal flows. Since then, several applications of the trapped-vortex concept have been considered, particularly as regards flow control around airfoils or wings, analysed through both theoretical/numerical studies [4–7] and experimental investigations [7, 8]. The trapped-vortex control applied to airfoils normally requires a steady large structure with almost constant vorticity to form in the cavity and to create a recirculation region separated from the outer flow by a thin and stronger shear layer [6]. The main difficulty of this approach is to obtain a strong and stable vortex inside the large cavity. In effect, it has been observed experimentally [7, 8] and shown by stability analysis [4] that stable vortices only seldom form inside the cavity, and an active control is therefore almost always necessary. For this reason, some control strategies have been proposed and tested. For instance, the possibility of controlling the flow over an airfoil through a trapped vortex combined with blowing and suction for its stabilization is studied experimentally in [8]. Regarding the trapped-vortex control applied to diffusers, a vortex-controlled diffuser that relies on the aerodynamic design of large cusps on the diffuser walls to locate vortices is described in [3]. Even though auxiliary devices, such as lips, vanes, secondary walls, are also used to facilitate the flow reattachment and the vortex formation, only limited success is obtained, due to the difficulty in having a stable vortex system. Indeed, it is demonstrated experimentally in [12] that the pressure recovery in a short diffuser can be enhanced only by an actively-stabilized trapped vortex (Cranfield diffuser).

On the other hand, the multi-step afterbody idea (see e.g. [10]) permits to obtain a reduction of the base drag of a bluff body. It consists in a number of backward facing steps placed upstream of the base; at each step a recirculation region derives from the separation and reattachment of the flow. These recirculations determine a configuration with a reduction in base area and in base suctions (as happens in a boat-tailed afterbody). To achieve the flow separation and reattachment at each afterbody step, a small step height should be chosen, of the same order as the boundary layer thickness. Therefore, these vorticity regions are smaller and weaker compared to the trapped vortices. The use of steps with curved contours to control separation and improve the performance of boat-tails was proposed in [11]. In spite of the preliminary nature of the numerical analysis, it was shown that efficient multi-step afterbodies may be obtained, provided the geometry of the steps is suitably chosen.

To our knowledge, the use of steps or cavities with contoured shapes has so far been proposed only for external flows. Conversely, in the present work we focus on boundary layer separation control in internal flows. As a paradigmatic example of a flow of technological interest, in which the control of separation could lead to beneficial effects, we consider a plane diffuser configuration. The design and the performance of plane diffusers have been rather extensively investigated in the literature, both in low Reynolds number conditions (see e.g. [13–19]) and at higher Reynolds numbers (see e.g. [20–22]).

Regarding the laminar flow regimes, which will be analysed in this work, the experimental investigations in [13, 14] show the different flow features

that can be found in a diffuser with a gradual or a sudden geometric expansion. These results are also confirmed in [15] through numerical analyses of two-dimensional straight-walled diffusers. From these works it is clear that very different flow topologies can be found in a diffuser. When the geometric expansion is gradual, with low divergence angle and low area-ratio, the flow is attached to the side walls and is symmetric to the centreline. When the divergence angle or the area ratio increases, an asymmetric flow recirculation can be observed along the diffuser, with separation occurring only on one side wall, while the flow on the other wall remains attached. By further increasing the divergence angle or the area ratio, a smaller secondary recirculation zone can be found on the wall opposite to that of the larger one, until, at very large divergence angles and area ratios, two recirculation regions occur in the diffuser: the flow separates at the beginning of the diffuser diverging walls on both sides, the sizes of the two recirculation regions are nearly identical and the flow remains symmetric. The Reynolds number is also crucial to determine which type of flow is present in a given diffuser configuration and the transition from one configuration to another (see e.g. [13, 19])).

In the present work, we use numerical simulations to investigate the effectiveness of the proposed control strategy, and choose to limit our analysis to low Reynolds numbers. In effect, laminar flow through geometric expansions has numerous engineering applications, especially in the field of microfluidics (see e.g. the review papers [23–25]); examples are the design of micropumps (see e.g. [17, 18]), electronic cooling systems and other heat-exchanging devices (see e.g. [26, 27]). Similar flow configurations are found also in biomedical problems (see e.g. [28]).

Moreover, for low Reynolds numbers turbulence can be neglected and this has some positive implications. First, from a practical point of view, such simulations require much lower computational costs than those at higher Reynolds, which need turbulence models. Moreover, errors due to numerical discretization can be made negligible, by checking the grid independence and the sensitivity to the used numerical schemes, and uncertainties due to turbulence models are obviously not present. Finally, it is well known that laminar boundary layers are less resistant to adverse pressure gradients than turbulent ones and, therefore, control methods successfully reducing or avoiding separation of laminar boundary layers may be expected to be effective also in the turbulent regime. Nonetheless, a final assessment of the results obtained in the present work also at higher Reynolds numbers, closer to those of many practical applications, would certainly be useful, and is postponed to future investigations. The aim of the present work is to find the optimal cavity shape and location, i.e. the ones producing the largest reduction in boundary layer separation and, hence, the largest increase in diffuser efficiency. Thanks to the reduced cost of the numerical simulations for the considered problem, a complete optimization is carried out considering four different parameters characterizing the location and the geometry of a couple of symmetric cavities. In particular, a question at issue is whether the optimal cavities are small (of the order of the boundary layer thickness) as in the multi-step afterbody concept, or large as for the trapped-vortex control. The robustness of the control to small modifications of the optimum cavity parameters is also addressed. Finally, the same diffuser-shape optimization is repeated for different operating conditions, obtained by modifying the inlet

boundary layer thickness.

2. Flow analysis for the reference diffuser configuration

2.1. Geometry definition

The considered diffuser geometry is made of a first part having constant width, a second one in which the width grows linearly and a final one having again constant width (see Fig. 1). These three parts are connected smoothly with roundings.

The diffuser is characterized by the following quantities: the inlet half-width, h (used here as reference length), the outlet half-width $k = 2h$, the length from the inlet to the beginning of the diverging part, $l_1 = 3h$, the length of the diffuser diverging part, $l_2 = 16.35h$, the length from the end of the diffuser diverging part to the end of the diffuser, $l_3 = 30.65h$, half of the divergence angle, $\alpha = 3.5°$, the curvature radius of the first rounding, $r_1 = 6h$, and the curvature radius of the second rounding, $r_2 = 6h$. The diffuser area ratio, i.e. the ratio between the diffuser outlet and inlet cross-areas, is $AR = 2$. Moreover, the total diffuser length is $l = (l_1+l_2+l_3) = 50h$.

The adopted frame of reference is shown in Fig. 1. Note that in all the figures dimensionless coordinates are used, i.e. $X = x/h$ and $Y = y/h$ (capital letters are used for dimensionless parameters and lowercase letters for dimensional quantities).

2.2. Simulation set-up and numerical methodology

The simulations are carried out at $Re = h \cdot u/\nu = 500$, where u is the x-velocity on the diffuser axis at the inlet section and ν the kinematic viscosity.

The inlet velocity field upstream of the diffuser is specified by using a Blasius boundary layer profile on the two walls with thickness $\delta_0 = 0.10h$; however, different values of δ_0/h are also considered (see Sec. 5.2).

For the simulations of the fluid flow inside the diffuser three different computational codes are used, namely Fluent, AERO and OpenFOAM. The numerical methodologies used by each code to solve the laminar Navier-Stokes equations are briefly described below, while further details may be found in [29].

Fluent (see e.g. [30]) is based on the finite-volume discretization method, and two-dimensional incompressible simulations have been carried out for the plane diffuser geometry. Unsteady time advancing is chosen together with a second-order implicit scheme. The adopted dimensionless time step is $\Delta T = \Delta t/(l/u) = 7 \times 10^{-4}$, and represents the ratio between the dimensional simulation advancing step Δt and the time necessary to a flow moving at velocity u to pass through the diffuser length l. A second-order upwind scheme is used for the space discretization. The segregated PISO algorithm (Pressure-Implicit with Splitting of Operators) is chosen to couple the pressure and momentum equations (see e.g. [31]). The computational grid is unstructured and is made of triangular elements.

AERO is an in-house developed code which uses a finite-element/finite-volume space discretization method applicable to three-dimensional unstructured grids. The AERO code considers compressible flows and transient simulations have been carried out for laminar compressible flow to reach the expected steady solution. An implicit second-order time advancing scheme is used. The adopted dimensionless time step is $\Delta T = 5 \times 10^{-3}$. A second-

order upwind scheme preconditioned for the low Mach regime is used for the space discretization (see e.g. [32]). Since the solver is compressible, the free-stream Mach number is chosen to be equal to 0.1 in order to make a sensible comparison with incompressible simulations. Moreover, the AERO solver requires a three-dimensional geometry, and thus, in order to obtain a 2D flow to be compared with the 2D simulation carried out by Fluent, the same unstructured 2D grid used with Fluent is extruded in the spanwise direction. The domain spanwise thickness is very small, equal to $0.1h$, and periodic boundary conditions are imposed in the spanwise direction. Moreover, after each simulation, the velocity component normal to the diffuser plane is evaluated in order to check that it is negligible, i.e. to check that the solution is really two-dimensional. This is a commonly used numerical procedure in order to obtain a 2D flow from a 3D solver. The results on the grid nodes laying on the mid-plane in the spanwise direction, i.e. in the plane at $z = 0$, are considered for comparison with the solutions obtained with the other codes.

Incompressible simulations have been carried out also with OpenFOAM (see e.g. [33]), an open-source code based on the finite-volume discretization method. The same numerical schemes and time step used for the Fluent simulations are chosen. The grid is false-three-dimensional, i.e. the two-dimensional plane diffuser grid, unstructured and made of triangular elements, is extruded along its normal direction. Thus, the volume elements are prisms with a triangular base. Periodic boundary conditions are imposed at the prism faces in the spanwise direction, as done for AERO. The results in the plane across the centroids of each cell, i.e. in the plane in the middle

of the diffuser spanwise direction, are considered.

In all the considered simulations, after a numerical transient the flow inside the diffuser becomes steady. For each solver, adequate sensitivity analyses have been carried out to reach the independence of the results from the grid resolution. In particular, 4 different grid resolutions have been considered in the $x-y$ plane, characterized by 9.47×10^4, 1.42×10^5, 2.34×10^5 nodes, and 4.25×10^5 nodes respectively. Grid independence was checked on the mean pressure recovery coefficient, defined in Eq. (1) in Sec. 2.3. The results obtained on the two finest grids showed a difference of less than 0.1%. Therefore, the 2D grid having 2.34×10^5 nodes was chosen for the analysis. For the simulations carried out with OpenFOAM and AERO the relative 3D grids were obtained, starting from this selected 2D grid, as previously explained.

2.3. Flow features and validation

The visualization of the flow streamlines in Fig. 2 shows that the diffuser is characterized by a large asymmetric zone of separated flow, which reattaches before the end of the diffuser. This flow configuration is bistable, i.e. the separation zone can develop on either side of the diffuser.

The diffuser performance is evaluated through the mean pressure recovery coefficient $\overline{C_p}$, which is defined as:

$$\overline{C_p} = \frac{\overline{p_{out}} - \overline{p_{in}}}{\frac{1}{2}\rho\overline{u_{in}}^2}, \tag{1}$$

where $\overline{p_{in}}$ and $\overline{u_{in}}$ are the area-weighted average pressure and x-velocity at the diffuser reference inlet section $X = 1$, $\overline{p_{out}}$ is the area-weighted averaged pressure at the diffuser outlet ($X = 50$). The reference section at $X = 1$ was

chosen to avoid nonphysical local pressure perturbations occurring at $X = 0$ due to the inlet boundary condition.

The performance of the diffuser is also evaluated through the efficiency η, defined as:

$$\eta = \frac{\overline{C_p}}{\overline{C_{p_{ideal}}}}, \tag{2}$$

where the ideal pressure recovery coefficient $\overline{C_{p_{ideal}}}$ is calculated as:

$$\overline{C_{p_{ideal}}} = 1 - \left(\frac{1}{AR}\right)^2 = 1 - \left(\frac{h}{k}\right)^2, \tag{3}$$

Thus, for this diffuser (with area ratio $AR = 2$) we have $\overline{C_{p_{ideal}}} = 0.75$.

A further parameter was used to evaluate the efficiency of the diffuser, namely the pressure recovery coefficient on the diffuser axis C_{p_a}, defined as:

$$C_{p_a} = \frac{p_{a_{out}} - p_{a_{in}}}{\frac{1}{2}\rho {u_{a_{in}}}^2} \tag{4}$$

where $p_{a_{in}}$, $p_{a_{out}}$ and $u_{a_{in}}$ are the pressure and the x-velocity values along the diffuser axis at the reference inlet and outlet sections.

The simulations are also compared by evaluating the mean pressure coefficient $\overline{C_{p_x}}$ at different sections along the length of the diffuser, which is defined as:

$$\overline{C_{p_x}} = \frac{\overline{p_x} - \overline{p_{in}}}{\frac{1}{2}\rho \overline{u_{in}}^2} \tag{5}$$

where $\overline{p_x}$ is the area-weighted averaged pressure at the considered X section of the diffuser.

The behaviour of $\overline{C_{p_x}}$ along the diffuser axis is shown in Fig. 3(a). It can be seen that there is an initial expansion due to the growth of the boundary layer thickness, which, inside the constant-section initial part of the diffuser, i.e. for $X \leq 3$, increases from the initial value $\delta_0 = 0.1h$ to $\delta_3 = 0.31h$.

In the diverging part of the diffuser the pressure increases, but the effect of separation is to slow down the rate of increase of $\overline{C_{p_x}}$ (compare Fig. 3(a) and Fig. 3(b)). Fig. 3(a) also shows that the different codes give consistent results. Indeed, the range of the diffuser pressure recovery coefficients is $\overline{C_p} = 0.386 - 0.389$ (0.386 for Fluent, 0.387 for OpenFOAM and 0.389 for AERO), with a consequent range of efficiency $\eta = 0.515 - 0.519$. As for the pressure recovery coefficient on the diffuser axis, the different codes give $C_{p_a} = 0.339 - 0.342$. Despite the different numerical approach and computational set-up of AERO compared to those of the other two codes, the discrepancies in the predictions of $\overline{C_p}$ and of the diffuser efficiency are lower than 0.8%.

The differences in the extension of the flow separation region predicted by the three codes are negligible, even if the extent of the separated region evaluated by using AERO is slightly smaller, which is consistent with the results for $\overline{C_p}$ and C_{p_a} (see Fig. 3(b)).

In the previously mentioned unsteady and pseudo-transient simulations, after a numerical transient the flow inside the diffuser becomes steady. Thus, a steady-state simulation was carried out by using Fluent, with the same schemes used for the unsteady Fluent simulation. The steady and the unsteady Fluent simulations gave the same results, in terms of pressure recovery and separation extent. Furthermore, the sensitivity to the coupling and discretization schemes was also studied and all the considered schemes gave very similar results (see [29]). Therefore, the following simulations and the optimization of the configurations with cavities were carried out by using Fluent to solve the steady two-dimensional discretized Navier-Stokes equations. Indeed, this method implies the lowest computational costs with respect to the

remaining ones, while providing the same accuracy.

3. Optimization of the diffuser shape

3.1. Optimization procedure

As a first step, the possible improvements of the diffuser efficiency that could be obtained only by optimizing the diffuser roundings were analysed. Therefore, a rounding shape optimization procedure was developed in order to maximize the pressure recovery in the diffuser and, hence, the efficiency parameter η (see Sec. 3.2). Subsequently, it was investigated whether larger efficiency improvements could be obtained by using cavities as passive flow-control devices in the diffuser with already-optimized roundings. A cavity optimization was carried out in order to identify the cavity shape which allows the diffuser efficiency to be maximized (see Sec. 4.1). These optimizations were carried out in the same operating conditions described in Sec. 2. The robustness of the results is then addressed in Sec. 5.1. The same diffuser-shape optimizations were finally repeated for different operating conditions, obtained by modifying the inlet boundary layer thickness (see Sec. 5.2).

The optimizations were carried out through an automatic procedure. In each optimization loop, the diffuser geometry is defined, the computational grid is generated and the cost function is evaluated through the numerical simulation of the flow inside the diffuser. The numerical results are managed by the optimization algorithm, which determines the modified configurations, finally leading to the optimized geometry. The optimization algorithm is the Multi-Objective Genetic Algorithm MOGA-II [34, 35], used herein with a single-objective function (see e.g. [36] for the use of MOGA-II in single-

objective optimization). This algorithm has been chosen for its robustness, because the complexity of the optimization problem was not known beforehand. In all cases, the parameter space is discretized in intervals of uniform size; an initial population is generated through a pseudo-random Sobol sequence [35], by using a subset of the specified discrete parameter values. The population evolves through the following reproduction operators: directional crossover, mutation and selection [35]. The probability of directional crossover, of mutation and of selection are set to 0.5, 0.1 and 0.05.

Different indexes of the diffuser efficiency could be chosen as the objective function in the optimization procedure, namely the maximization of the section-averaged pressure recovery coefficient $\overline{C_p}$, the maximization of the pressure recovery coefficient on the diffuser axis C_{p_a}, or the minimization of the total dissipation inside the diffuser. The parameter $\overline{C_p}$, which is equivalent to the efficiency parameter η, was chosen as the objective function, because its evaluation has a smaller computational cost compared to that of the total dissipation and represents a good index of the diffuser performance. Nonetheless, after the optimization, the dissipation and the pressure recovery coefficient on the diffuser axis C_{p_a} were also evaluated in order to have a further confirmation of the results.

While $\overline{C_p}$ and C_{p_a} have been already defined in equations (1) and (4), the role of the dissipation function becomes clear by referring to the following form of the integral equation of the kinetic energy balance:

$$\int_V \frac{\partial \rho \left(\frac{V^2}{2}\right)}{\partial t} dV + \int_S \rho \left(\frac{V^2}{2}\right) \mathbf{V} \cdot \mathbf{n} dS =$$

$$-\int_S p\mathbf{V}\cdot\mathbf{n}dS+\int_S \tau_{\mathbf{n}}\cdot\mathbf{V}dS-\int_V \Phi dV \tag{6}$$

where the three integrals on the right-hand side represent, respectively, the work done on the fluid, in unit time, by the pressure and viscous forces acting on the volume boundary S and the total dissipation within the volume V of fluid bounded by surface S.

Since the diffuser flow is steady (see Sec. 2) and the work done on the fluid by the viscous forces acting on the boundary is negligible compared to that of the pressure forces ($\mathbf{V}=0$ along the diffuser walls while the integral representing the total work of the viscous forces is very small at the inlet and outlet compared to the one connected with the pressure forces), the kinetic energy balance becomes:

$$\int_S \rho\left(\frac{V^2}{2}+\frac{p}{\rho}\right)\mathbf{V}\cdot\mathbf{n}dS=-\int_V \Phi dV \tag{7}$$

Equation (7) highlights that the dissipation is immediately connected with the balance of the kinetic and pressure energy in the flow, i.e. not all the kinetic energy variation is converted into pressure energy because of the viscous losses. Thus, the minimum of the total dissipation is expected to be found in the diffuser configuration with an optimized efficiency.

For an incompressible flow, the total dissipation Φ_t in a volume V may be easily obtained as a function of the enstrophy ω^2 (the square of vorticity) present in the volume and the acceleration $\mathbf{a}$ at its boundary, through the Bobyleff-Forsyth formula (see e.g. [37], [38] and [39]):

$$\Phi_t=\int_V \Phi\, dV=\mu\int_V \omega^2\, dV+2\mu\int_S \mathbf{a}\cdot\mathbf{n}\, dS \tag{8}$$

3.2. Optimization of the reference configuration

An optimization of the diffuser roundings is carried out in order to maximize $\overline{C_p}$ and, hence, the efficiency η, in the reference configuration without cavities. The optimization parameters are the non-dimensional radii of the roundings at the beginning and at the end of the diffuser diverging walls, respectively r_1/h and r_2/h (see Fig. 1). They are varied from 0, i.e. a sharp-edged configuration, to 120. The parameter space is discretized by using a uniform interval of size equal to 1, i.e. 120×120 discrete parameter values are explored by the MOGA-II algorithm. The initial population was composed of 15 individuals, distributed in the discretized parameter space by means of the previously cited Sobol sequence. Then, 4 additional generations were created by the optimization algorithm, each one composed of 15 individuals. A summary table with the geometries and the results of all the simulations is reported in [29]. Starting from the third generation, most of the new individuals created by the algorithm are characterized by $r_1/h = 0$ and by values of r_2/h in a neighborhood of 0 (11 over 15 individuals in the fourth generation), which correspond to the highest values of the objective function. Moreover, the maximum value of the objective function reached in the third and fourth generation varies by 0.1%. Therefore, the resulting optimum solution is characterized by sharp edges ($r_1/h = 0$ and $r_2/h = 0$) instead of roundings. However, the use of sharp edges leads to an increase in $\overline{C_p}$, and thus in efficiency η, of only 1.7% compared to the reference configuration having roundings $r_1/h = 6$ and $r_2/h = 6$ (as shown in Fig. 4(a), $\overline{C_p}$ increases from 0.386 to 0.393 in the sharp-edged diffuser configuration). The analysis of the pressure recovery coefficient on the diffuser axis C_{p_a} and of

the total dissipation Φ_t inside the diffuser confirms these results. An increase of C_{p_a} from 0.339 to 0.345 and a reduction of the total dissipation from 0.212 to 0.209 are indeed found in the optimum-shape diffuser configuration (note that in this paper the dimensionless values of Φ_t, obtained by using the inlet reference quantities, are reported).

In effect, as may be deduced from Fig. 4(a), sharp edges at the beginning of the diffuser diverging walls allow a slightly larger pressure recovery to be obtained in the first part of the diffuser. On the other hand, the use of sharp edges does not significantly modify the extent of the separated region (see Fig. 4(b)). Probably this result is due to the fact that, at the considered low Reynolds number, the boundary layer thickness approaching the edge is so thick that roundings have no beneficial effects, and this also explains the small gain in diffuser efficiency obtained by the basic optimization of the diffuser shape taking only the roundings into account.

4. Diffuser with contoured cavities

4.1. Optimization of the cavity shape in the diffuser with sharp edges

The proposed flow-control method is used in the diffuser with already-optimized roundings, i.e. in the sharp-edged diffuser configuration, to investigate whether cavities are able to further improve the diffuser efficiency and to reduce the extent of the separated region. One couple of symmetric cavities is positioned on each side of the diffuser. The cavities start with a sharp edge, have an upstream part with a semi-elliptical shape, and end with a spline tangent to the diffuser diverging walls (see Fig. 5).

The previously described optimization procedure has been used to determine the optimum shape of the cavities that maximizes the pressure recovery $\overline{C_p}$. The optimization variables are: the distance from the beginning of the diffuser diverging part to the upstream edge of the cavity, s/h, the cavity total length, t/h, the ellipse axis parallel to the diffuser diverging wall, a/h, and the ellipse axis normal to the diffuser diverging wall, b/h.

The upstream edge of the cavity and its ending point are allowed to vary along all the diffuser diverging walls, while the considered range for both axes of the cavity is from one-fifth to four-times the inlet boundary layer thickness, i.e. from $0.02h$ to $0.4h$. The parameter space was discretized by using uniform intervals having a width of 0.01, 0.01, 0.1 and 0.2 for a/h, b/h, s/h and t/h respectively. The initial population was composed of 25 individuals, distributed in the discretized parameter space by means of the previously cited Sobol sequence. Then, 7 additional generations were created by the optimization algorithm, each one composed of 25 individuals. A summary table with the geometries and the results of all the simulations is reported in [29]. Starting from the sixth generation, most of the new individuals created by the algorithm are characterized by $s/h = 0$, $b/h = 0.12 - 0.13$ and $t/h = 11.2 - 12.8$ (8 over 25 individuals in the seventh generation), which, as explained in the following, correspond to the highest values of the objective function. Moreover, the maximum value of the objective function reached in the sixth and seventh generation varies by 0.2%.

Suitably-shaped cavities lead to a successful control of boundary layer separation. A pressure recovery increase of 13.0% was found compared to the sharp-edged diffuser without cavity ($\overline{C_p}$ increases from 0.393 to 0.444 in

the configuration with optimum cavities). The pressure recovery coefficient on the diffuser axis C_{p_a} and the total dissipation Φ_t inside the diffuser also confirm the optimization results. An increase of the C_{p_a} from 0.345 to 0.390 (+13.0%) and a reduction of the dissipation from 0.209 to 0.187 (-10.5%) are indeed found.

An unsteady simulation of the flow inside the diffuser with optimized cavities was carried out, to check that the flow is stable even after the introduction of the contoured cavities in the diffuser diverging walls. The result was found to coincide with the one of the steady-state simulation.

From the visualization of the streamlines in the diffuser with optimized cavities, sketched in Fig. 6, it is evident that the flow separates at the cavity edge but reattaches immediately downstream, forming a recirculation region; furthermore, the subsequent asymmetric flow separation is delayed and its extent is reduced. The reasons of the reduction of the separated flow region and of the improvement of the diffuser performance will be more deeply analysed in Sec. 4.2.

Regarding the optimum cavity parameters, the ellipse axis normal to the diffuser diverging walls b/h and the upstream edge of the cavity s/h are the most important parameters. Indeed, the maximum value of $\overline{C_p}$ is obtained for a well defined value or in a narrow range of values of these parameters, namely $b/h = 0.12 - 0.13$ and $s/h = 0$. As will be explained in depth in Sec. 5.1, b/h is very significant because it determines the width of the recirculation region and, thus, the possibility of having a reattachment of the flow after the cavities. The optimum value of b/h is definitely smaller than the thickness of the boundary layer at the start of the diverging part of

the diffuser, i.e. $b/\delta_3 = 0.39 - 0.42$, and it is about equal to the displacement thickness ($\delta_3^*/h = 0.102$). This suggests that the present control device is more closely related to the multi-step afterbody concept than to the use of large trapped vortices. The optimum value of s/h is the minimum one allowed by the geometric constraints imposed in the optimization, i.e. in this case the presence of the sharp edges; thus, the cavities start at $X = 3$. The cavity total length t/h is also very important. All the optimum cavities end approximately at the beginning of the asymmetric separation zone, i.e. $t/h = 11.2 - 12.8$. However, it should be noticed that, since the cavities end tangent to the diffuser diverging walls, the geometries included in this t/h range are very similar and practically can be considered to almost coincide. Conversely, the ellipse axis parallel to the diffuser diverging walls, a/h, has an almost negligible effect. The range of the parameter a/h within which the optimum value of the objective function is reached is large ($a/h = 0.30 - 0.38$) and it will be seen in Sec. 5.1 that it may be further extended.

An additional cavity optimization was carried out in order to identify the cavity shape which allows the efficiency to be maximized in the diffuser configuration with roundings $r_1/h = r_2/h = 6$. The results show that the flow control device is effective also in this diffuser configuration (see [29]), with an improvement of the diffuser efficiency of the order of 10.9%. The pressure recovery coefficient on the diffuser axis C_{p_a} and the total dissipation Φ_t inside the diffuser also confirm the optimization results. Indeed, C_{p_a} increases by 10.9%, while Φ_t decreases by 8.5%.

It should be noted that the use of optimized cavities in the sharp-edged diffuser leads to an efficiency gain that is definitely greater than the one

obtained by using them in the diffuser with roundings. In effect, for the sharp-edged diffuser with optimized cavities the efficiency increases by 15% compared to the diffuser configuration with roundings and without cavities, i.e. the original configuration of the diffuser. Thus, sharp edge and cavities can be successfully used together to increase the pressure recovery inside the diffuser. The improvement of the flow-control device effectiveness obtained by combining cavities and sharp edges is mainly due to the fact that the cavity can start immediately after the edges, rather than at the end of the roundings, and advancing the beginning of the cavity produces a significant increase in pressure in the first part of the diffuser diverging walls, where the cavities are placed.

4.2. Analysis of the mechanisms leading to enhanced diffuser performance

A deeper analysis of the velocity and vorticity fields in the region where the cavities are introduced was carried out to investigate on the main mechanisms through which the boundary layer separation is delayed and the pressure recovery performance of the diffuser is improved.

First of all, it is evident from Fig. 6 that the optimized configuration is characterized by the presence of a closed recirculation region in which the velocity remains very low (not shown for the sake of brevity), and by a main stream flowing outside it. Therefore, the outer streamlines adjacent to the boundary of the recirculation zone are also modified by the presence of the cavity. Hence, one may wonder whether the favourable effect produced by the optimized cavity might also be obtained through a geometry modification of the diffuser lateral surfaces causing an analogous modification of the flow streamlines. A simulation was then carried out with a diffuser in which the

streamline bounding the recirculation region of the optimized cavity flow was replaced by a solid surface. This produced a diffuser with a modified geometry, characterized by a rapid increase of the cross section in the region that actually bounds the recirculation, followed by a long portion with slightly reduced divergence angle compared to the original diffuser. This new geometry may be considered as an additional output of the procedure leading to the optimized cavities.

The modified diffuser without cavities does indeed produce a performance improvement over the original reference configuration. However, although this improvement is significant, it does not reach the values of the diffuser with optimized cavities. In fact, the resulting value of $\overline{C_p}$ is 0.429, with a 9.1% increase over the reference value, compared to the 13% gain for the diffuser with optimized cavities. Correspondingly, a reduction in dissipation of 7.25% is found, and should be compared to the value of 10.5% for the diffuser with optimized cavities. The results obtained for the modified diffuser are compared in more detail with those of the reference configuration and of the diffuser with optimized cavities in Figs. 7(a) and 7(b), where the variations of $\overline{C_{p_x}}$ along the three diffusers are shown together with the corresponding extents of the separation regions. As can be seen, compared to the reference configuration, there is a larger increase in pressure at the beginning of the diffuser diverging part for both the modified diffuser and the one with the optimized cavities, due to the local geometry modifications. More downstream, the pressure losses are lower than in the reference configuration due to a reduction of the separated region extent. This latter effect is clearly more pronounced for the diffuser with cavities, which is the case

caracterized by the smallest separated flow region.

In order to gain a deeper insight on the reason of these results, the streamwise variation of the integral of the enstrophy ω^2 over cross-sections at constant X, which is denoted by ϕ, is shown in Fig. 8 for the three configurations. As can be seen from the Bobyleff-Forsyth formula (8), this quantity gives the contribution of each cross-section to the dissipation in the diffuser. In effect, the last term in Eq. (8) is zero at the lateral walls and almost negligible at the first and last cross-sections of the diffuser. The figure shows that, compared to the original diffuser, the value of ϕ is significantly lower in the diffusers with cavities and with modified geometry, with the sole exception of a small region corresponding to the beginning of the optimized cavity. Furthermore, it is also clear that in the cross-sections corresponding to the recirculation region the contribution to dissipation is lower in the diffuser with cavities than in the one with modified lateral walls.

This behaviour is clearly related to the vorticity distribution of the different configurations in the region where the geometry modifications are introduced. In particular, Fig. 9 shows the lateral profiles of vorticity along three cross-sections of the diffusers which correspond to the beginning, the middle and the end of the recirculation region of the optimized cavity flow (see Fig. 6). At the lateral coordinates that are common to the three configurations, the vorticity values of the diffuser with cavities are significantly lower than those of the other configurations. Obviously, vorticity is present also in the region inside the cavity, where it shows a decreasing trend which finally leads to small negative values, in agreement with the changed direction of the velocity near the cavity wall. As for the diffuser with modified geometry, the

relevant near-wall vorticity is higher than the one of the basic diffuser in the region corresponding to the beginning of the cavity, but becomes lower more downstream.

From the above results, it may be deduced that the main mechanism responsible for the positive effect of the contoured cavities is a reduction of the loss of momentum in the near-wall region. In detail, the improvement of the diffuser performance seems to be due both to the modification of the streamlines of the flow outside the recirculation zone, which can be seen as a virtual geometry modification, and to a reduced dissipation. As previously observed, the global increase in pressure recovery is thus caused by the concentrated pressure increase due to the sudden widening of the diffuser cross-section, which is common to the diffuser with cavities and to the one with modified geometry, and to a reduction of the extent of the subsequent boundary layer separation, which is more significant for the diffuser with cavities, probably due to the lower associated dissipation. In a sense, compared to the diffuser with modified geometry, the main effect of the cavity seems to be the relaxation of the no-slip boundary condition along the contour of the recirculation region, which leads to lower momentum losses.

A final observation deriving from the above analysis, and in particular from Fig. 9, is that the region inside the contoured cavities does not correspond to a local concentration of vorticity, but rather to a zone where vorticity is reduced compared to the one that is present in the original configuration. Therefore, this region cannot really be described as a trapped vortex, which, conversely, is characterized by a comparatively large region with almost constant vorticity surrounded by thin and strong shear layers

(see [6]). The present flow within and immediately downstream of the cavity may rather be compared to the separation bubble occurring behind a backward-facing step whose height is smaller than the thickness of the incoming boundary layer, as in the multi-step afterbody concept.

5. Sensitivity to changes in parameters and flow conditions

5.1. Robustness analysis of the optimized flow control device

In this section the effects of some cavity modifications are investigated, in order to ascertain whether this flow control device is robust with respect to small variations of the cavity parameters from the optimum ones. First of all, we focus on the ellipse axis normal to the diffuser diverging walls b/h, which has been identified as the most important parameter because it determines the width of the recirculation region produced by the cavity. The robustness of the flow-control device to the parameter b/h is analysed by varying it in the range $0.04 - 0.28$; as for the other parameters, s/h and t/h are kept fixed to their optimum values, i.e. $s/h = 0.0$, $t/h = 12.0$, while a/h is varied in the range $0.20 - 0.33$, considering its negligible effect.

The efficiency gains remain significant for small changes of the cavity shape parameters around the optimum value. In the range $b/h = 0.08 - 0.15$ the proposed configuration is robust, because the efficiency increments are always above 11% compared to the reference diffuser (see Fig. 10). In practice, an improvement of $\overline{C_p}$ with the increase of the normal cavity height is found as long as the flow reattaches immediately downstream of the recirculation region produced by the cavity, until the optimum value is reached, i.e. $b/h = 0.12 - 0.13$. For all values of b/h below the optimal one, the

performance of the diffuser with cavities is better than the one of the diffuser without cavities (see Fig. 11) and the pattern of the streamlines is similar to the one of the optimum configuration, even if with a slightly larger separation zone (see Fig. 12). Conversely, above the optimum value there is an abrupt decrease of the diffuser $\overline{C_p}$, because the flow on one side of the diffuser becomes completely separated (see Fig. 13 and Fig. 14). Therefore, for sufficiently large values above the optimal ones of b/h the diffuser efficiency may become even worse than the one of the diffuser without cavities. The evaluation of the total dissipation Φ_t inside the diffuser confirms the trends outlined above for the optimization results. Indeed, the dissipation decreases as long as the flow reattaches downstream of the cavity, while an increase of Φ_t is found when one side of the diffuser is completely separated (see Fig. 10).

Regarding the parameter s/h, the optimum cavities start at the beginning of the diffuser diverging walls, i.e. $s/h = 0$. The robustness of the flow-control device to the parameter s/h is analysed by increasing it to 0.1 and 0.2, while the other cavity parameters are kept fixed to their optimum values. Increasing s/h leads to a reduction of the pressure recovery $\overline{C_p}$ in the first part of the diffuser (see Fig. 15(a)) and, thus, to a reduction of the diffuser efficiency. Indeed, the streamline starting from the cavity upstream edge and separating the recirculation region from the external flow moves downstream (see Fig. 15(b)). On the other hand, the three cavities give the same reduction of the separated region (see Fig. 15(c)). Thus, the increments of the efficiency are, respectively, +12.0% for $s/h = 0.1$ and +11.2% for $s/h = 0.2$.

As regards the cavity total length t/h, the optimized cavities end approximately at the beginning of the asymmetric separation zone. The value of t/h is then varied in the range $6.0 - 16.0$, in order to evaluate the robustness of the flow-control device to variation of its value, while the other parameters, s/h and b/h are kept fixed to their optimum values, i.e. $s/h = 0.0$, $b/h = 0.12$. The results are shown in Fig. 16. Small increases of the parameter t/h do not cause a significant reduction in efficiency because, since the cavity ends tangent to the diffuser diverging walls, the shapes of the cavity for all the t/h values above the optimal one are very similar. On the other hand, a reduction of t/h determines a decrease of $\overline{C_p}$, due to an early and unnecessary local reduction of the diffuser cross section. These trends are confirmed also by the evaluation of the dissipation function Φ_t.

As already pointed out, the ellipse axis parallel to the diffuser diverging walls a/h is not a significant parameter for the optimization of the flow control device. Therefore, instead of carrying out a robustness analysis with respect to this parameter, we focus on the effect of its elimination, i.e. we put $a/h = 0$. Thus, the semi-elliptical cavity is replaced by a step normal to the diffuser diverging walls, with a height equal to the previously defined optimum value of the parameter b/h (see Fig. 17). The results obtained with the two different geometries are very close; indeed, in the diffuser with the step an increase in pressure recovery of 12.7% was found. By comparing Figs. 17 and 6(b), it may be seen that, in effect, a similar recirculation region is present in the two cases. Moreover, an unsteady simulation of the flow inside this diffuser geometry was carried out to verify whether the flow is stable even after the introduction of the step, and the result was found to be equal to

the one of the steady-state simulation. Thus, from a fluid-dynamical point of view, the two configurations work in a similar way and, therefore, the choice between them may be determined by manufacturing requirements.

5.2. Optimization of the cavity shape in different operating conditions

In this section the effect of the modification of the inlet boundary layer thickness on the flow control device performance is investigated. The inlet boundary layer thickness is modified in the range $\delta_0/h = 0 - 0.20$, using a uniform interval of size equal to 0.05, while the Reynolds number is kept constant, i.e. $Re = 500$ (based on the inlet velocity on the axis, u, and the length h). Note that this implies that the average inlet velocity $\overline{U_{in}} = \overline{u_{in}}/u$ decreases with increasing boundary layer thickness (see Table 1).

Although the operating conditions change, the behaviour of $\overline{C_{p_x}}$ along the diffuser axis in all cases without cavities is similar to that shown in Fig. 3(a). There is an initial expansion due to the growth of the boundary layer thickness, which, inside the constant-section initial part of the diffuser, i.e. for $X \leq 3$, increases from the initial value of δ_0 to δ_3. In the same part of the diffuser the displacement thickness also increases from δ_0^* to δ_3^* (see Table 1). In the diverging part of the diffuser the pressure increases, and the effect of separation is to slow down the rate of increase of $\overline{C_{p_x}}$. The diffuser configurations without the cavities are always characterized by a steady asymmetric flow, similar to the one described in Sec. 3.2.

A slight reduction of the separated region extent with the reduction of δ_0/h is found. Indeed, when δ_0/h decreases, the boundary layer has a larger momentum near the wall and, therefore, the condition of flow separation is slightly delayed and reduced. The reduction of the separation produces

δ_0/h	$Case$	δ_3/h	δ_3^*/h	$\overline{U_{in}}$	$\overline{C_p}$	η	C_{p_a}	Φ_t
0.00	Reference	0.27	0.090	1.000	0.393	0.524	0.364	0.233
0.00	Optimum	0.27	0.090	1.000	0.446	0.595	0.413	0.207
0.05	Reference	0.29	0.097	0.982	0.393	0.524	0.354	0.221
0.05	Optimum	0.29	0.097	0.982	0.445	0.593	0.400	0.197
0.10	Reference	0.31	0.102	0.963	0.393	0.524	0.345	0.209
0.10	Optimum	0.31	0.102	0.963	0.444	0.592	0.390	0.187
0.15	Reference	0.33	0.110	0.946	0.397	0.530	0.341	0.199
0.15	Optimum	0.33	0.110	0.946	0.448	0.598	0.384	0.179
0.20	Reference	0.35	0.116	0.928	0.402	0.536	0.336	0.189
0.20	Optimum	0.35	0.116	0.928	0.453	0.604	0.379	0.171

Table 1: Summary of all the optimum results

an increase of the pressure recovery on the axis $p_{a_{out}} - p_{a_{in}}$ and, since the velocity on the axis is the same in all the operating conditions, of the pressure coefficient on the axis C_{p_a}. The trend of $\overline{C_p}$, instead, is not as clear as the one of C_{p_a}, because in this case also the dimensionless value of the area-weighted averaged x-velocity $\overline{U_{in}}$ at the diffuser inlet section increases with the reduction of δ_0/h and δ_3/h. Thus, $\overline{C_p}$ is the ratio between the pressure recovery $\overline{p_{out}} - \overline{p_{in}}$ and the dynamic pressure $\frac{1}{2}\rho\overline{u_{in}}^2$, which both increase with the reduction of δ_0/h and δ_3/h (see Table 1); consequently, the variations of $\overline{C_p}$ with boundary layer thickness are significantly smaller than those of C_{p_a}.

The same flow-control-device optimization described in Sec. 4.1 was repeated for the different operating conditions. In all the considered cases, suitably-shaped cavities lead to increases in $\overline{C_p}$ of $12.7\% - 13.5\%$, compared

to the sharp-edged diffuser without cavities in the same conditions (see Table 1). Furthermore, in all cases the boundary layer separation point is delayed and the separated region extent is significantly reduced. The improvements are confirmed by the reduction of the dissipation found in the optimum configurations. As might be expected, the variations of $\overline{C_p}$ and Φ_t are always in opposite correlation.

The parameters characterizing the optimum cavities are summarized in Table 2. Again, the ellipse axis normal to the diffuser diverging walls, b/h, has a great importance because it determines the width of the steady recirculation region produced by the cavity; moreover, the optimum cavities start as soon as possible ($s/h = 0$) and they end approximately at the beginning of the asymmetric separation zone (parameter t/h). Conversely, the ellipse axis parallel to the diffuser diverging walls, a/h, has a very small effect also in these operating conditions.

It should be noted that the optimum values of the ellipse axis normal to the diffuser diverging walls are found to be very close even for the different inlet boundary layer thicknesses, i.e. $b/h = 0.12 - 0.13$. The optimum cavity height is definitely smaller than the thickness of the boundary layer at the start of the diverging part of the diffuser, i.e. $b/\delta_3 = 0.35 - 0.45$, and it is of the order of the displacement thickness δ_3^*/h. Furthermore, as found in Sec. 5.1, the proposed configurations are robust to small changes of all the parameters around their optimum values as long as the flow reattaches immediately downstream of the cavities. In particular, the efficiency gains remain above 11% in the range $b/h = 0.08 - 0.15$ (see [29]).

δ_0/h	s/h	t/h	b/h
0.00	0.0	16.0	$0.12 - 0.13$
0.05	0.0	$14.0 - 15.2$	$0.12 - 0.13$
0.10	0.0	$11.2 - 12.8$	$0.12 - 0.13$
0.15	0.0	$11.0 - 12.2$	$0.12 - 0.13$
0.20	0.0	$10.0 - 12.0$	$0.12 - 0.13$

Table 2: Summary of all the optimum parameters

6. Conclusions

In the present work a passive control of boundary layer separation in a two-dimensional symmetrical diffuser has been developed and investigated. The control method consists in modifying the geometry of the diffuser walls using contoured cavities with suitable shape. The final goal is to increase the pressure recovery inside the diffuser by delaying the flow separation and reducing its extent.

The laminar flow inside a two-dimensional plane diffuser having an area ratio of 2 and a total divergence angle of 7 degrees has been investigated. The Reynolds number is $Re = 500$, based on the diffuser half-width at the inlet section and the inlet velocity on the axis. Numerical simulations were first carried out in the reference diffuser configuration, i.e. without the flow control device, using three different codes, and an almost negligible sensitivity of the simulated flows to the numerics was ascertained. Therefore, the code and algorithms implying the lowest computational cost with comparable accuracy were used in the subsequent analyses.

Even if a symmetrical velocity-inlet profile is used, the flow in the diffuser is characterized by a steady, albeit bistable, asymmetric zone of separated flow.

One cavity was then introduced on each side of the diffuser diverging walls and an optimization was carried out in order to identify the cavity shape allowing the pressure recovery, and thus the diffuser efficiency, to be maximized. The cavities start with a sharp edge at the beginning of the diverging portion of the diffuser, have an upstream semi-elliptical shape and end with a spline curve tangent to the diffuser walls. The cavity geometry was defined by using four parameters, namely the cavity starting point, its total length and the two ellipse axes.

The use of suitably-shaped cavities leads to a significant reduction of boundary layer separation in the diffuser, and to an increase in efficiency of the order of 13%. The improvement in the diffuser performance is also confirmed by the pressure recovery coefficient on the diffuser axis C_{p_a} and by the evaluation of the total dissipation inside the diffuser.

In the diffuser configuration with optimized cavities the flow separates at the cavity upstream edge and rapidly reattaches, forming a closed recirculation region within and immediately downstream of the cavities. This produces a local widening of the diffuser cross-section and a consequent enhanced increase of the pressure coefficient. Furthermore, the reduction of the subsequent asymmetric separation zone compared to the original configuration contributes to a decrease of the associated pressure losses. A simulation was also performed of the flow inside a modified diffuser with solid lateral walls coinciding with the streamlines bounding the recirculation regions that

are produced by the optimized cavities. The results of the comparison between the various configurations and the analysis of the vorticity field showed that both the new "virtual geometry" of the diffuser and the reduced contribution to dissipation in the near-wall region are responsible for the good performance of the diffuser with cavities, whose efficiency improvement is always higher than the one provided by the modified diffuser.

A robustness analysis of the flow-control device showed that the efficiency improvements remain significant also for small changes of the cavity shape parameters around the optimum ones. The ellipse axis normal to the diffuser diverging walls, b/h, turned out to be the most important parameter, because it determines the width of the steady recirculation region produced by the cavity. An improvement of $\overline{C_p}$ with the increase of b/h occurs as long as the flow reattaches immediately downstream of the cavities. However, above this value there is an abrupt reduction of the diffuser efficiency because the flow on one side of the diffuser becomes completely separated.

An important output of the present analyses is that the optimum cavity height is definitely smaller than the thickness of the boundary layer at the start of the diverging part of the diffuser. Thus, the present control device is more closely related to the multi-step afterbody concept than to the idea of producing large trapped vortices contained within cavities whose typical dimensions are much larger than the thickness of the upstream boundary layer.

Finally, it was found that the length of the ellipse axis parallel to the diffuser diverging walls a/h is not a critical parameter in the optimization. In practice, if required by manufacturing constraints, the cavity semi-ellipse

can be replaced by a simple step normal to the diffuser diverging walls with a height equal to b/h without a significant decrease of the diffuser performance.

In the last part of the work, the same optimization procedure has been repeated for different operating conditions, obtained by modifying the inlet boundary layer thickness in the range $\delta_0/h = 0 - 0.20h$. Also in these cases, suitably-shaped cavities were found to lead to a successful control of the boundary layer separation in the diffuser. Indeed, the use of these passive control devices provides increments in the $\overline{C_p}$ of about 13%, compared to the sharp-edged diffuser without cavities in the same conditions. Once again, the boundary layer separation point is delayed and the separated region extent is significantly reduced by the presence of the optimized cavities. As for the parameters characterizing the optimum cavities, their range of values and relative importance are similar in all conditions.

In future investigations, the performance of contoured cavities in increasing the efficiency of diffusers with different divergence angles and at higher Reynolds numbers will be analysed.

References

[1] M. Gad-el-Hak, Modern development in flow control, Applied Mechanical Reviews 49 (1996) 365–379.

[2] J. C. Lin, Review of research on low-profile vortex generators to control boundary-layer separation, Progress in Aerospace Sciences 38 (4-5) (2002) 389–420.

[3] F. Ringleb, Separation control by trapped vortices, in: Lachmann, G.V.

(Ed.), Boundary layer and flow control, Vol. 1, Pergamon Press, Oxford (1961) 265–294.

[4] A. Iollo, L. Zannetti, Trapped vortex optimal control by suction and blowing at the wall, European Journal of Fluid Mechanics B-Fluids 20 (2001) 7–24.

[5] S. I. Chernyshenko, B. Galletti, A. Iollo, L. Zannetti, Trapped vortices and a favourable pressure gradient, J. Fluid Mech. 482 (2003) 235–255.

[6] R. Donelli, S. Chernyshenko, P. Iannelli, A. Iollo, L. Zannetti, Flow models for a vortex cell, AIAA Journal 47(2) (2009) 451–467.

[7] W. F. J. Olsman, T. Colonius, Numerical simulation of flow over an airfoil with a cavity, AIAA Journal 49 (1) (2011) 143–149.

[8] D. Lasagna, R. Donelli, F. De Gregorio, G. Iuso, Effects of a trapped vortex cell on a thick wing airfoil, Exp Fluids 51 (2011) 1369–1384.

[9] J. A. C. Kentfield, Short, multi-step, afterbody fairings, J. Aircraft 21 (5) (1984) 351–352.

[10] P. R. Viswanath, Flow management techniques for base and afterbody drag reduction, Prog in Aerospace Sci. 32 (1996) 79–129.

[11] G. Buresti, D. Tondi, Stepped boat-tails: a proposal for the control of the aerodynamic loads on bluff bodies, Atti del Dipartimento di Ingegneria Aerospaziale, ADIA 2007-7, ETS Editrice, Pisa (2007).

[12] R. C. Adkins, A short diffuser with low pressure loss, Journal of Fluid Engineering, ASME 93 (1975) 297–302.

[13] F. Durst, A. Melling, J. H. Whitelaw, Low reynolds number flow over a plane symmetric sudden expansion, J. Fluid Mech. 64 (1974) 111–128.

[14] Y. Y. Tsui, C. K. Wang, Laminar flow calculation in planar diffusers, Proceedings of the 18th National Conference on Theoretical and Applied Mechanics, Hsinchu, Taiwan (1994).

[15] Y. Y. Tsui, C. K. Wang, Calculation of laminar separated flow in symmetric two-dimensional diffusers, Journal of Fluids Engineering 117 (1995) 612–616.

[16] T. Suzuki, T. Colonius, S. Pirozzoli, Vortex shedding in a two-dimensional diffuser: theory and simulation of separation control by periodic mass injection, Journal of Fluid Mechanics 520 (2004) 187–213.

[17] V. Singhal, S. V. Garimella, J. Y. Murthy, Low Reynolds number flow through nozzle-diffuser elements in valveless micropumps, Sensors and Actuators A 113 (2004) 226–235.

[18] Y. C. Wang, J. C. Hsu, P. C. Kuo, Y. C. Lee, Loss characteristics and flow rectification property of diffuser valves for micropumps applications, International journal of Heat and Mass Transfer 52 (2004) 328–336.

[19] M. Nabavi, Three-dimensional asymmetric flow through a planar diffuser: Effects of divergence angle, reynolds number and aspect ratio, International Communications in Heat and Mass Transfer 37 (2010) 17–20.

[20] R. S. Azad, Turbulent flow in a conical diffuser: A review, Experimental Thermal and Fluid Science 13(4) (1996) 318–337.

[21] K. Kibicho, A. T. Sayers, Benchmark experimental data for fully stalled wide-angled diffusers, Journal of Fluids Engineering 130 (2008) 1–4.

[22] S. M. El-Behery, M. Hamed, A comparative study of turbulence models performance for separating flow in a planar asymmetric diffuser, Computer and Fluids 44 (2011) 248–257.

[23] P. Gravesen, J. Branebjerg, O. S. Jensen, Microfluidics - a review, Journal of Micromechanics and Microengineering 3(4) (1993) 168–182.

[24] S. Shoji, M. Esashi, Microflow devices and systems, Journal of Micromechanics and Microengineering 4(4) (1994) 157–171.

[25] V. Singhal, S. Garimella, A. Raman, Microscale pumping technologies for microchannel cooling systems, Applied Mechanics Reviews 57(1-6) (2004) 191–221.

[26] H. K. Ma, B. Hou, C. Lin, J. Gao, The improved performance of one-side actuating diaphragm micropump for a liquid cooling system, Int. Commun. Heat Mass Transf. 35 (2008) 957–966.

[27] M. Thiruvengadam, B. Armaly, J. A. Drallmeier, Three-dimensional mixed convection in plane symmetric sudden expansion, Int. J. Heat Mass Transfer 52 (2009) 899–907.

[28] M. R. Kaazempur-Mofrad, S. Wada, J. G. Myers, C. R. Ethier, Mass

transport and fluid flow in stenotic arteries: axisymmetric and asymmetric models, Int. J. Heat Mass Transfer 48 (2005) 4510–4517.

[29] A. Mariotti, A. N. Grozescu, G. Buresti, M. V. Salvetti, A passive method for flow separation control: application to a 2d diffuser configuration, Atti del Dipartimento di Ingegneria Aerospaziale, ADIA 2012-1, ETS Editrice, Pisa (2012).

[30] ANSYS Fluent, Help system, Fluent 6.3 user's guide, ANSYS, Inc. (2006).

[31] R. I. Issa, Solution of the implicit discretized fluid flow equations by operator splitting, Journal of Computational Physics 65 (1) (1986) 40–65.

[32] S. Camarri, M. V. Salvetti, B. Koobus, A. Dervieux, A low-diffusion muscl scheme for les on unstructured grids, Computers and Fluids 33 (2004) 1101–1129.

[33] OpenFOAM, Openfoam 1.6 user's guide, www.openfoam.org (2009).

[34] S. Poles, Y. Fu, E. Rigoni, The effect of initial population sampling on the convergence of multi-objective genetic algorithms, Multiobjective Programming and Goal Programming, Springer Berlin Heidelberg 3 (2009) 123–133.

[35] ModeFrontier, Modefrontier user's guide (version 4.0), www.esteco.com (2009).

[36] S. Poles, E. Rigoni, T. Robic, MOGA-II performance on noisy optimization problems, Proceedings of the International Conference on Bioinspired Optimization Methods and their Applications, Jozef Stefan Institute, Ljubljana (2004) 51–62.

[37] J. Serrin, Mathematical principles of classical fluid mechanics, in: Flügge S. (Ed.), Handbuch der Physik VIII/1, Springer-Verlag, Berlin (1959) 125–263.

[38] G. Buresti, Notes on the role of viscosity, vorticity and dissipation in incompressible flows, Meccanica 44 (2009) 469–487.

[39] G. Buresti, Elements of Fluid Dynamics, Imperial College Press, London, 2012.

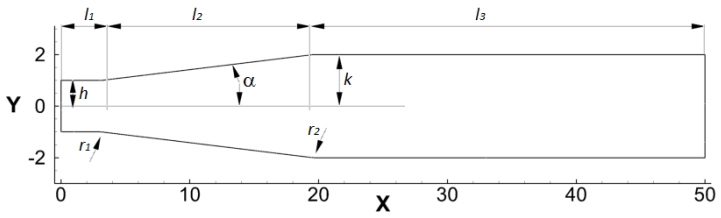

Figure 1: Diffuser geometry and reference frame

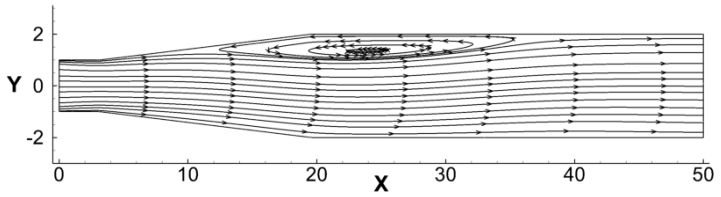

Figure 2: Streamlines inside the diffuser

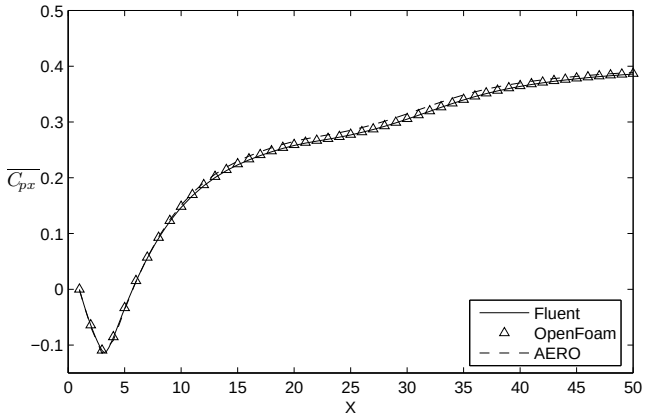

(a) Mean pressure coefficient at different X sections

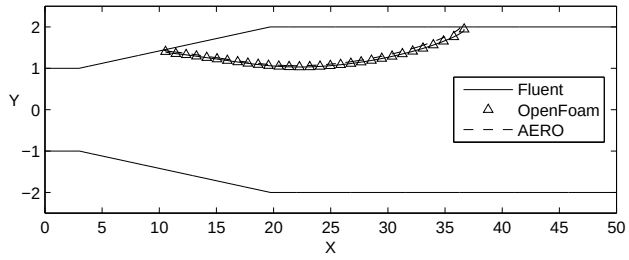

(b) Separated region extent

Figure 3: Mean pressure coefficient and separated region extent for the reference diffuser

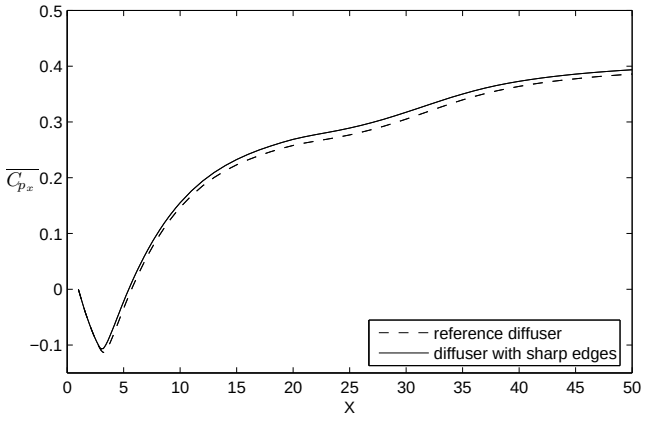

(a) Mean pressure coefficient at different X sections

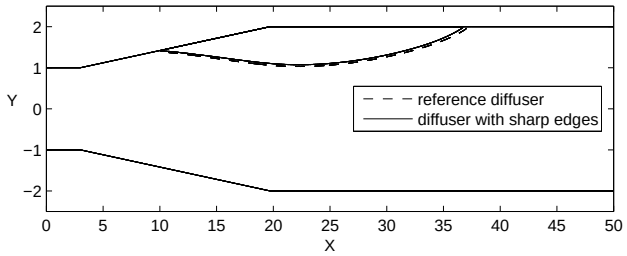

(b) Separated region extent

Figure 4: Comparison between the reference diffuser and the shape-optimized one

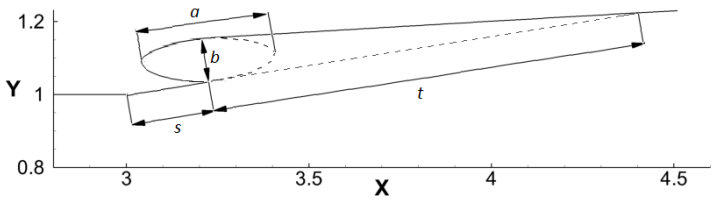

Figure 5: Parameters to be optimized

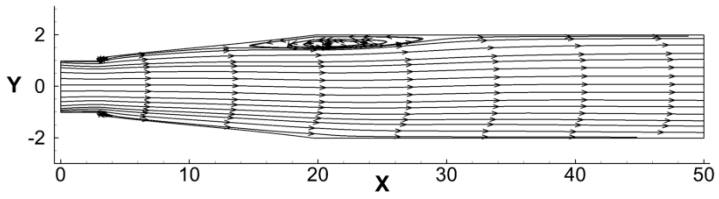

(a) Diffuser with optimized cavities

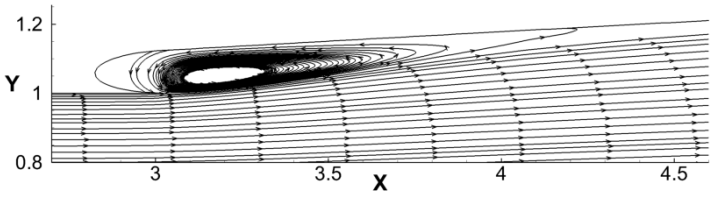

(b) Streamlines inside the optimized cavity

Figure 6: Streamlines in the diffuser with optimized cavities

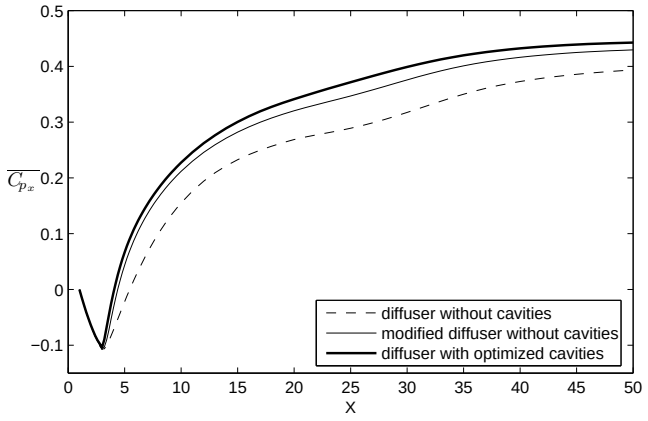

(a) Mean pressure coefficient at different X sections

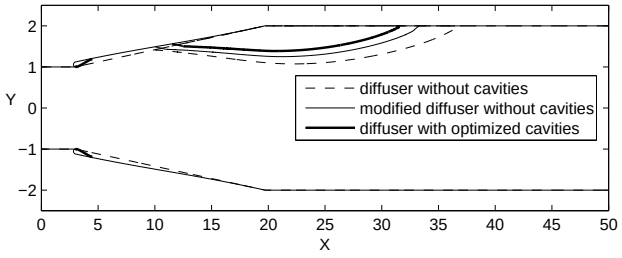

(b) Separated region extent

Figure 7: Mean pressure coefficient and separated region extent; comparison between the diffuser without cavities, the modified diffuser without cavities and the diffuser with optimized cavities

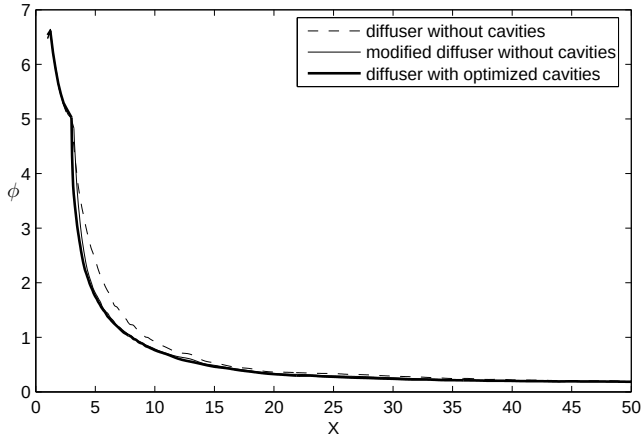

(a) Integral of enstrophy

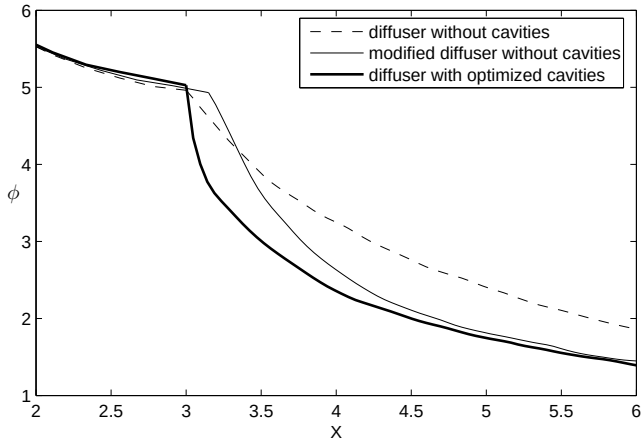

(b) Integral of enstrophy - zoom

Figure 8: Integral of enstrophy along the diffuser width at different X sections

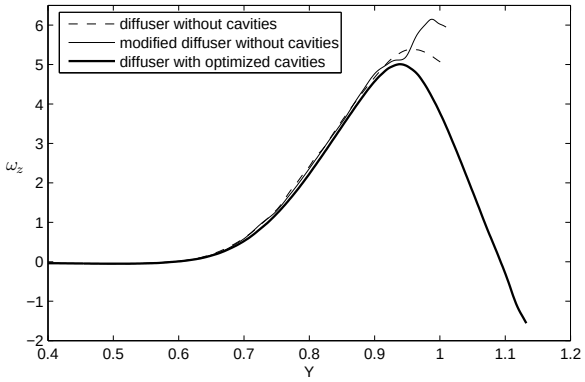

(a) $X = 3.2$

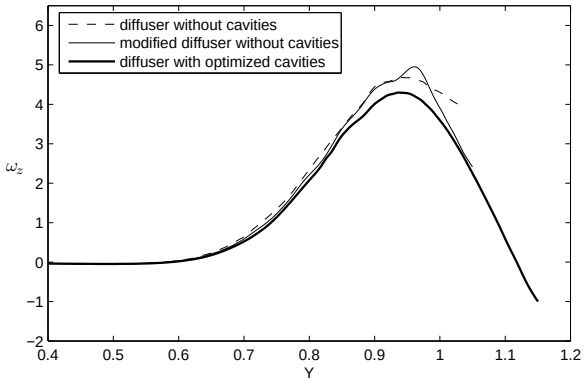

(b) $X = 3.5$

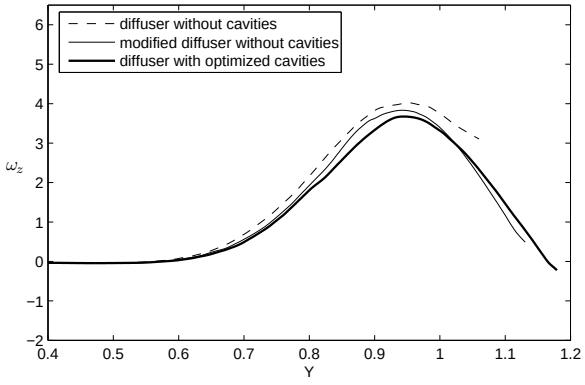

(c) $X = 4.0$

Figure 9: Vorticity profiles at different X sections

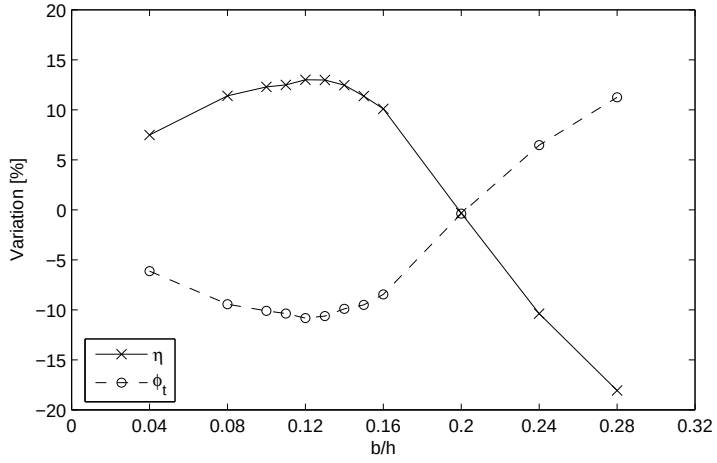

Figure 10: Effect of the variation of the parameter b/h

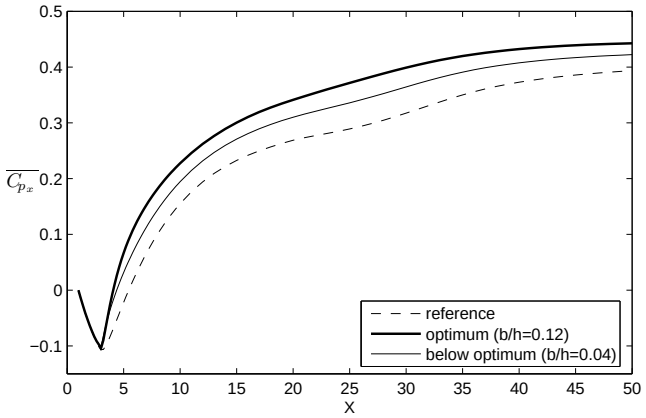

(a) Mean pressure coefficient at different X sections

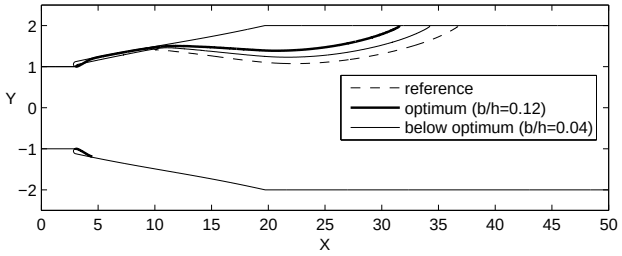

(b) Separated region extent

Figure 11: Results for values of the parameter b/h below the optimal one

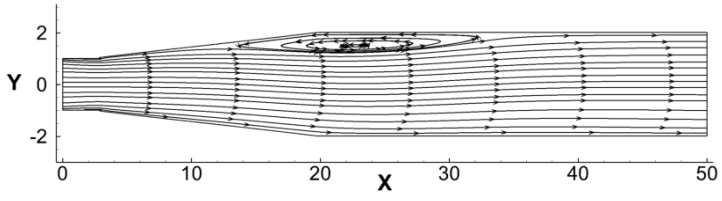

Figure 12: Streamlines for values of the parameter b/h below the optimal one

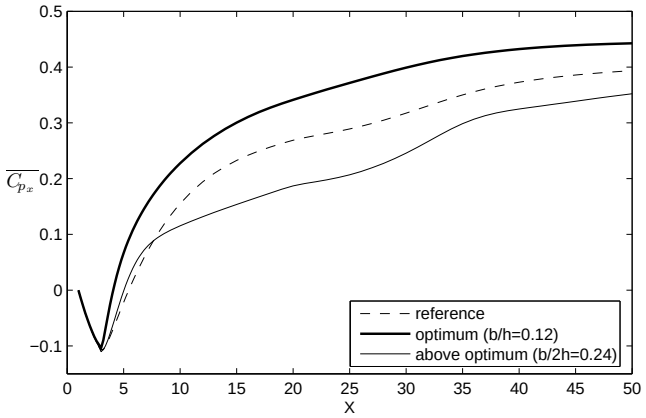

(a) Mean pressure coefficient at different X sections

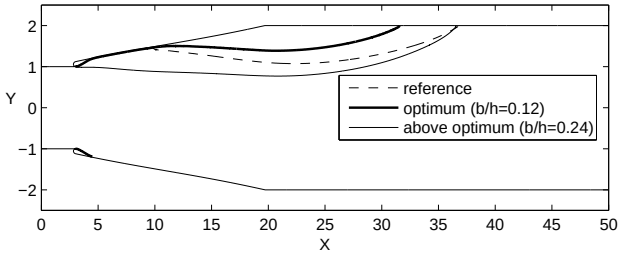

(b) Separated region extent

Figure 13: Results for values of the parameter b/h above the optimal one

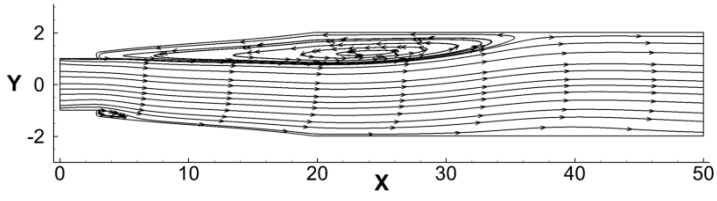

Figure 14: Streamlines for values of the parameter b/h above the optimal one

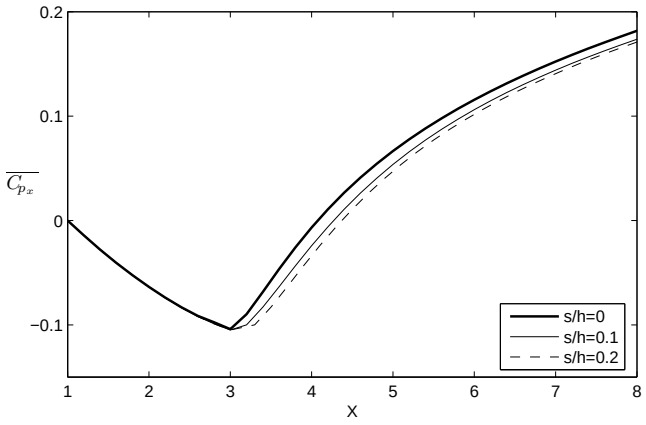

(a) Mean pressure coefficient at different X sections

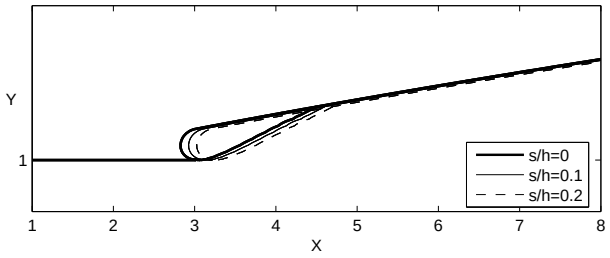

(b) Streamline separating the recirculation region produced by the cavity from the external flow

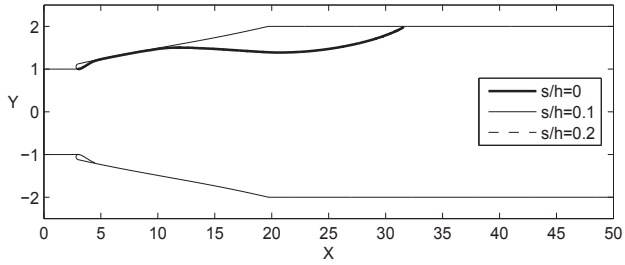

(c) Separated region extent

Figure 15: Effect of the variation of the parameter s/h

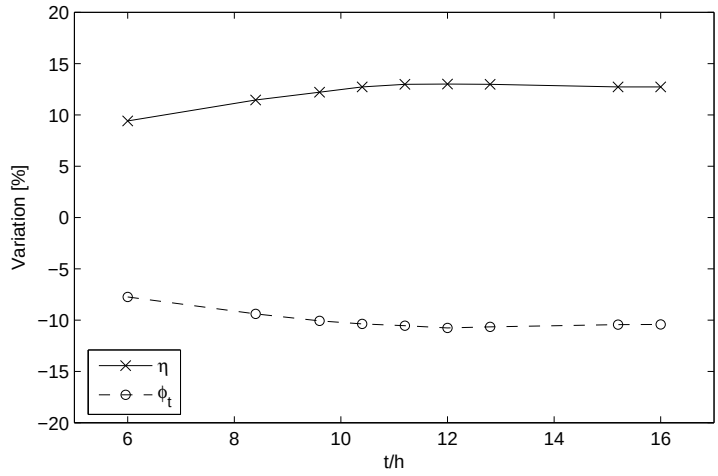

Figure 16: Effect of the variation of the parameter t/h

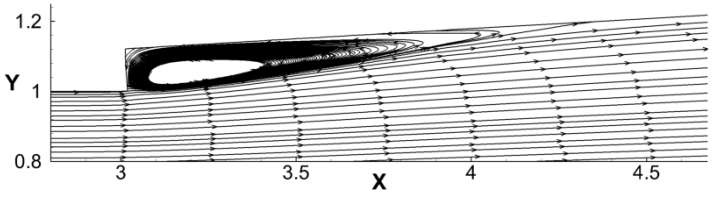

Figure 17: Effect of the cavity semi-ellipse elimination